A Real-time Compact Structured-light based Range Sensing System

Byung-Joo Hong, Chan-Oh Park, Nam-Seok Seo, and Jun-Dong Cho

***Abstract*—In this paper, we propose a new approach for compact range sensor system for real-time robot applications. Instead of using off-the-shelf camera and projector, we devise a compact system with a CMOS image-sensor and a DMD (Digital Micro-mirror Device) that yields smaller dimension (168x50x60mm) and lighter weight (500g). We also realize one chip hard-wired processing of projection of structured-light and computing the range by exploiting correspondences between CMOS image-sensor and DMD. This application-specific chip processing is implemented on an FPGA in real-time. Our range acquisition system performs 30 times faster than the same implementation in software. We also devise an efficient methodology to identify a proper light intensity to enhance the quality of range sensor and minimize the decoding error. Our experimental results show that the total-error is reduced by 16% compared to the average case.**

***Index Terms*—Range sensing, structured-light, FPGA**

I. INTRODUCTION

Recently, there have been several researches based on structured-light in order to acquire accurate range information [1], relying on a set of bulky projector and camera [2, 3]. One important application is smart robots that must recognize ambient surroundings autonomously using the structured-light. In this paper, we develop a compact range sensing system with a CMOS image-sensor and a DMD (Digital Micro-mirror Device), and provide an FPGA solution of the entire processing of range sensor system, i.e., projecting the structured-light patterns followed by computing the sensing range.

The generic range measurement system based on structured-light is as shown in Fig. 1. First, a projector generates the structured-light patterns that contain identifiable lines. A line on the image plane of the projector creates a light plane containing the center of projection and the projected line. Then, a camera captures the projected pattern onto a scene and identifies the lines generated by the projector. An image point on the image plane of the camera creates a light ray (camera ray) containing the center of projection and the projected point. The intersection of the plane and the ray yields the range information.

Generally, single-pattern structured-light encoding method is suitable for moving scenes, yet yielding low accuracy range data. Whereas multiple-pattern structured-light encoding method can acquire accurate distance data,

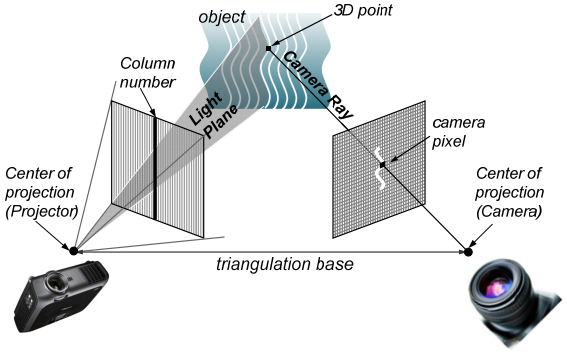

Fig. 1. Structured-light based range sensing [4].

Manuscript received Sep. 1, 2011; revised Nov. 8, 2011.
Sungkyunkwan University - Department of Electronic and Electrical Engineering, Suwon 440-746, Korea, Republic of
E-mail : jdcho@skku.edu

yet being vulnerable to the moving object [5]. Motivated by these facts, our approach is to apply high-speed CMOS image-sensor (500fps) and hard-wired range computation to overcome the vulnerability problem of the multiple pattern approach. Furthermore, we attain real time processing of dynamic scenes without losing accuracy.

To enhance the quality of range sensor and minimize the decoding error, we also present a methodology to identify a proper light intensity. There are related efforts which aim to enhance the quality of range sensor with adaptation to the scene. In [6] the authors introduced an adaptive algorithm with adjusting the coding patterns depending on the environment. However, there is no flexibility with structured-light coding methods due to the specially designed coding patterns. In [7] the authors presented an adaptive algorithm with using the partially reconstructed scene. However, this approach is not suitable for real-time application due to its high computational complexity although it provides high accuracy results. In this paper, we present a methodology to enhance the quality of range sensor in real time with adjusting the light intensity according to the suggested structured-light decoding error model.

The rest of the paper is organized as follows. In Section II, we shall exhibit the overall system architecture, and describe the process of structured-light decoding and ray-plane intersection. In Section III, we present on the error-minimized light intensity search. In Section IV, we will show our implementation and experimental results. Finally, Section V will conclude the paper.

II. SYSTEM ARCHITECTURE

As shown in Fig. 2, our architecture performs: 1) Structured-light patterns are projected by DMD, and captured by CMOS image-sensor. 2) The captured images are stored in external memory and decoded. 3) The decoded images are triangulated with the ray-plane intersection. 4) The final range data is transmitted to the external main control component through USB.

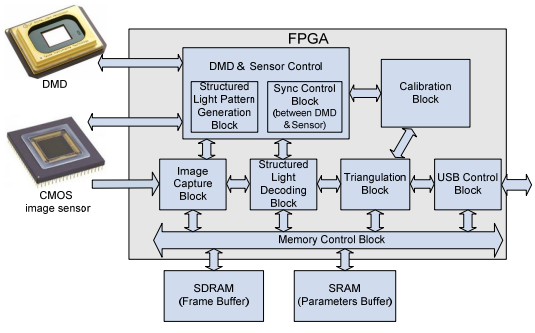

Fig. 2. The overall architecture of our system.

1. Structured Light Decoding

Structured-light decoding is a process of finding correspondences between the columns of the DMD projected pattern and the pixels of the captured image. We use Gray code for structured-light encoding. Gray code is well suited for binary position encoding due to its one bit difference property. More robust encoding is to add an inverted Gray pattern between two Gray patterns [8], as shown in Fig. 3.

The structured-light decoding process is shown in Fig. 4. We need one frame of non-illuminated image (i.e., reference image) and 16 frames of patterned images to decode the structured-light patterns. Each layer contains two frames; original Gray coded pattern and inverted Gray coded pattern. The decoding process is as follows. First, the pixel values of the patterned images are subtracted by the pixel value of the non-illuminated image (referred to 'Ref-frame-value'). The 'Frame value' represents the pixel value at each frame. The 'Frame value*' represents the value subtracted by the 'Ref-frame-value'. Next, we compare the 'Frame value*' between two 'Frame values' in each layer and choose the greater value (Layer value).

The 'Max frame#' bit is set to '0' if the left frame value (i.e., the pixel from the gray pattern) is greater than the right frame value (i.e., the pixel from the inverted gray pattern); otherwise set to '1'. All of the 'Max frame#' bits for all layers correspond to the index of the LUT (look-up table). The LUT yields the corresponding column of the projection image at the specific pixel of captured image. To remove the ambiguous decoding

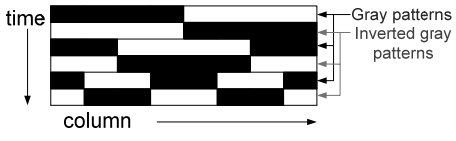

Fig. 3. The structure of sequence frames.

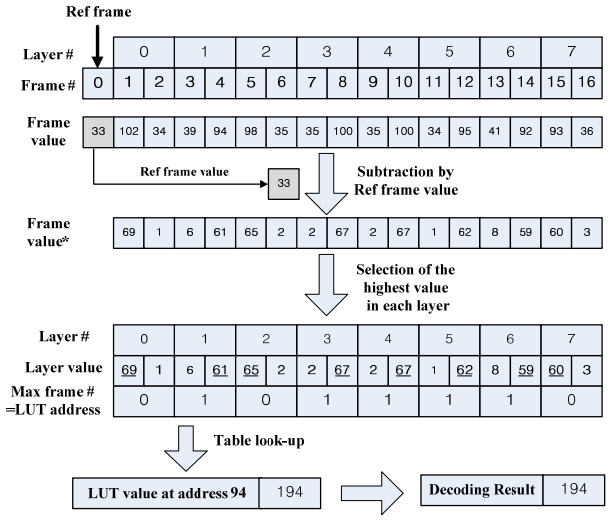

Fig. 4. Structured-light decoding process.

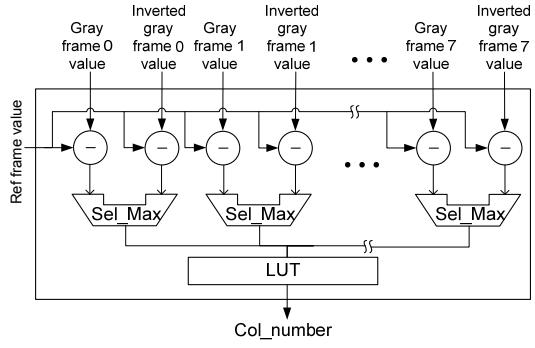

Fig. 5. Structured-light decoding hardware.

result, we reject the decoding result if 'Layer value' is less than the structured-light decoding threshold value (denoted as th_{sl}).

The above-mentioned decoding is structured as shown in Fig. 5. The 16 images are subtracted by the reference image. The pixel from the gray pattern and the pixel from the inverted gray pattern are compared. The compared result is an index of the LUT. The LUT also provide flexibility in using other structured-light encoding methods.

2. Ray-Plane Intersection

In the calibration process of the system, we determine the calibration parameters such as the focal distance, translation, and orientation of DMD and CMOS image-sensor. The calibration procedure is similar to the classical stereo-vision system with modeling a projector as an inverse-camera [9]. We triangulate with ray-plane

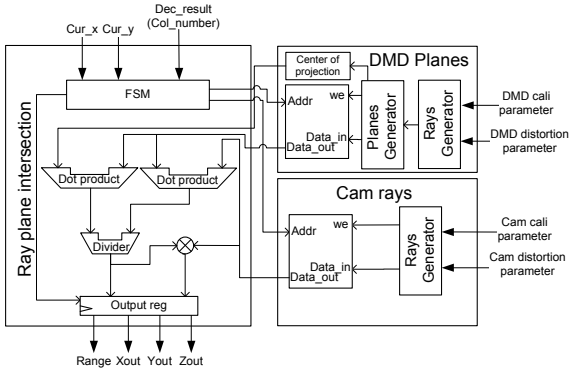

Fig. 6. Ray-plane intersection hardware.

intersection to yield the range. The DMD's center of projection and each column of DMD projected image form a plane. The image point and the center of the projection of image-sensor form a ray. We calculate rays and planes with the pre-calibrated DMD and image-sensor calibration parameters. The intersection point between the ray and the plane is the location of a point in the 3D world.

The range via ray-plane intersection can be represented as:

$$\text{range} = \frac{\mathbf{n}^{\mathbf{t}} \cdot \mathbf{p}}{\mathbf{n}^{\mathbf{t}} \cdot \mathbf{r}}, \tag{1}$$

where $\mathbf{n}^{\mathbf{t}}$ is a normal vector of a plane, $\mathbf{p}$ is a center of projection of DMD, and $\mathbf{r}$ is a ray vector.

Fig. 6 shows the hardware architecture of the above-mentioned operation.

III. Error Minimized Light Intensity Search

1. Defining Structured-light Decoding Error

Motivated by the fact that the quality of range sensor requires a proper light intensity, we specify the structured-light decoding error which can affect the distance results. We found that the error can be mainly categorized into two cases. One is the case where the decoding result is '0' (referred to as "*zero-error*"), and the other is the case where the initial order of encoded result is altered after decoding (referred to as "*order-error*"). The *'zero-error'* represents the number of range data. And the *'order-error'* implies the number of

uncertain range data. The zero-error can be classified into three cases such as "*zero-over-error*," "*zero-under-error*," and "*zero-occlusion-error*".

We explain on how to compute the above mentioned four different errors. The *zero-error* occurs when any '*Layer value*' (as shown in Fig. 4) is smaller than 'th_{sl}' at a pixel. That implies that the pixel value difference between light illuminated case and light non-illuminated case is smaller than 'th_{sl}'. This case occurs generally when we take the image of a dark object (e.g., black object) due to its low reflectivity.

For this case, we define the *zero-under-error*. This error can be changed depending on the intensity of the light γ in Eq. (2). The *zero-error* for pixel (*i,j*) is defined when the pixel value of structured-light decoding image (denoted as $I_{dec}(i,j,\gamma)$) is zero. The *zero-under-error* pixel is defined when the pixel value of reference image (denoted as $I_{ref}(i,j,\gamma)$) is less than (*255-*th_{sl}) in Eq. (3). In Eq. (3), the pixel value of *zero-under-error* image (denoted as $I_{zue}(i,j,\gamma)$) becomes '1'. Then, we get *zero-under-error* $\mathrm{E_{zue}}(\gamma)$ with counting all the 1's in $I_{zue}(i,j,\gamma)$ and with normalizing by the size of image (H × W).

$$\mathrm{E_{zue}}(\gamma) = \frac{1}{\mathrm{H\times W}}\sum_{\mathrm{i=1}}^{\mathrm{H}}\sum_{\mathrm{j=1}}^{\mathrm{W}} \mathrm{I_{zue}}(\mathrm{i,j},\gamma) \tag{2}$$

$$\mathrm{I_{zue}}(\mathrm{i,j},\gamma) = \begin{cases} 1 \text{ for } \mathrm{I_{dec}}(\mathrm{i,j},\gamma) = 0 \text{ and} \\ \mathrm{I_{ref}}(\mathrm{i,j},\gamma) < (255 - \mathrm{th_{sl}}) \\ 0 \text{ else} \end{cases} \tag{3}$$

Next, we define the *zero-over-error*. The *zero-error* also increases with increasing light intensity when we take image of a bright object (e.g., white object). The pixel value in this case is almost 255 without providing the projector's light. This causes smaller difference value than th_{sl}, due to the upper limited pixel value (255 for 8bit pixel resolution). We define this case as *zero-over-error*. In other words, we identify the *zero-over-error pixel* when the pixel value of reference image $I_{ref}(i,j,\gamma)$ is larger than *(255-*th_{sl}*)*. Similar to the *zero-under-error*, we define *zero-over-error* as shown in Eqs. (4, 5).

$$\mathrm{E_{zoe}}(\gamma) = \frac{1}{\mathrm{H\times W}}\sum_{\mathrm{i=1}}^{\mathrm{H}}\sum_{\mathrm{j=1}}^{\mathrm{W}} \mathrm{I_{zoe}}(\mathrm{i,j},\gamma) \tag{4}$$

$$\mathrm{I_{zoe}}(\mathrm{i,j},\gamma) = \begin{cases} 1 \text{ for } \mathrm{I_{dec}}(\mathrm{i,j},\gamma) = 0 \text{ and} \\ \mathrm{I_{ref}}(\mathrm{i,j},\gamma) > (255 - \mathrm{th_{sl}}) \\ 0 \text{ else} \end{cases} \tag{5}$$

Then, we define *zero-occlusion-error*. The *zero-error* also occurs when the pixel of captured image is in shadow area or out of sight from the projection area. We define this case as *zero-occlusion-error*. We identify *zero-occlusion-error pixel* when the pixel value difference between all-illuminated image (denoted as $\mathrm{I_{all}}(\mathrm{i,j},\gamma)$) and reference image $\mathrm{I_{ref}}(\mathrm{i,j},\gamma)$ is less than the threshold value (denoted as $th_{occlusion}$).

$$\mathrm{E_{zoce}}(\gamma) = \frac{1}{\mathrm{H\times W}}\sum_{\mathrm{i=1}}^{\mathrm{H}}\sum_{\mathrm{j=1}}^{\mathrm{W}} \mathrm{I_{zoce}}(\mathrm{i,j},\gamma) \tag{6}$$

$$\mathrm{I_{zoce}}(\mathrm{i,j},\gamma) = \begin{cases} 1 \text{ for } \mathrm{I_{dec}}(\mathrm{i,j},\gamma) = 0 \text{ and} \\ \mathrm{I_{all}}(\mathrm{i,j},\gamma) - \mathrm{I_{ref}}(\mathrm{i,j},\gamma) < (\mathrm{th_{occlusion}}) \\ 0 \text{ else} \end{cases} \tag{7}$$

Last, we define *order-error*. Among the valid decoding pixels (i.e., *non-zero-error pixels*), the decoded pixel value would contain error. The decoding result should be increased along the right direction since the decoding result corresponds to the column number of projector's image plane. We define the out-of-ordered decoding result error as *order-error*. We distinguish *order-error* for a pixel (*i,j*) by checking if the pixel value of the decoding image $I_{dec}(i,j,\gamma)$ is less than the pixel value of pre-positioned pixel $I_{dec}(i-1,j,\gamma)$. If $I_{oe}(i,j,\gamma) = 1$, then this case is out-of-order. Then, we accumulate the number of *order-error pixel* while $\mathrm{I_{oe}}(\mathrm{i,j},\gamma) = 1$, as shown in Eq. (8).

$$\mathrm{E_{oe}}(\gamma) = \frac{1}{1-\mathrm{E_{zet}}(\gamma)}\frac{1}{\mathrm{H\times W}}\sum_{\mathrm{i=1}}^{\mathrm{H}}\sum_{\mathrm{j=1}}^{\mathrm{W}} \mathrm{I_{oe}}(\mathrm{i,j},\gamma) \tag{8}$$

$$\mathrm{I_{oe}}(\mathrm{i,j},\gamma) = \begin{cases} 1 \text{ for } \mathrm{I_{dec}}(\mathrm{i,j},\gamma) < \mathrm{I_{dec}}(\mathrm{i}-1,\mathrm{j},\gamma) \\ 0 \text{ else} \end{cases} \tag{9}$$

We normalize to get the ratio of the *order-error* pixels to the non-zero-error pixels. Here, *zero-error-total* (denoted as $E_{zet}(\gamma)$) is defined as in Eq. (10).

$$\mathrm{E_{zet}}(\gamma) = \mathrm{E_{zoe}}(\gamma) + \mathrm{E_{zue}}(\gamma) + \mathrm{E_{zoce}}(\gamma) \tag{10}$$

Then, we finally get the total error as below.

$$E_{total}(\gamma) = E_{zet}(\gamma) + \omega_{oe} \cdot E_{oe}(\gamma), \quad (11)$$

where, ω_{oe} is the order-error-weight.

Finally, we find the optimum light intensity value (denoted as O_γ) among γ values so as to minimize the *total-error*.

$$O_\gamma = \arg\min_\gamma E_{total}(\gamma) \quad (12)$$

As shown in Fig. 7, we tested the error function depending on the intensity of the light. Our experiments reveal that the maximum light intensity (100%) does not always yield a good result. The *order-error* is much smaller than *zero-error* due to the reasonable structured-light encoding method. Even though the *order-error* is resided in a small value region as shown in Fig. 8, the error seems to be getting higher in some special case for the weak scene (i.e., transparent object and/or a mirror) for structured-light based range sensing system. To emphasize *order-error*, we assign a higher weight (ω_{oe}) on the $E_{oe}(\gamma)$ as shown in Eq. (11).

We determine ω_{oe} according to the relation between *zero-error* and *order-error* functions. When ω_{oe} = 1, the minimal $E_{total}(\gamma)$ light intensity is almost same as the minimal $E_{zet}(\gamma)$ light intensity, because the *zero-error* is dominant to the total-error. However, as ω_{oe} increases, the minimal $E_{total}(\gamma)$ light intensity varies to minimize the order-error. In this case, the minimal $E_{total}(\gamma)$ light intensity goes far from the minimal $E_{zet}(\gamma)$ light intensity and the number of 3D points

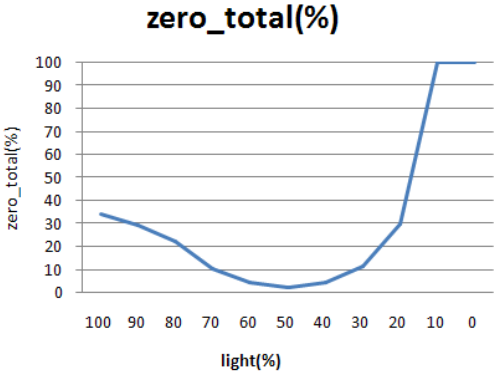

Fig. 7. *Zero-error* function (depending on the light intensity).

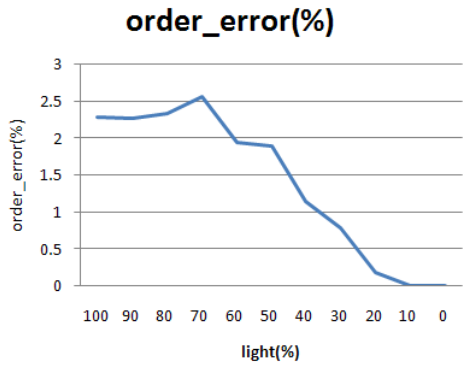

Fig. 8. *Order-error* function (depending on the light intensity).

decreases as the accuracy increases. Therefore, there is a tradeoff between the accuracy and the number of 3D points. In this paper, we determine ω_{oe} to 3 after experimentally analyzing the increasing rate of accuracy and decreasing rate of the number of 3D points, depending on ω_{oe}. When ω_{oe} is more than 3, we shall lose many 3D points with getting a little higher accuracy.

2. Light Intensity Search to minimize the decoding error

Light intensity search is done in an iterative manner as shown in Fig. 9. We search from 100% to 20% of light intensity with step size of 5%. The search process is performed to obtain the minimum error value (i.e., optimal light intensity) via capturing and examining a number of structured-light decoding images by employing different light intensity. For simplicity, we use the exhaustive search algorithm in this paper, and are in the process of developing the sophisticated algorithm to find the optimum light intensity with the minimum number of scans.

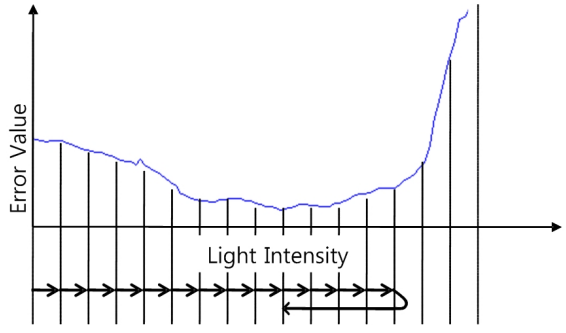

Fig. 9. Light Intensity Search.

3. Hardware Implementation of Error Estimation and Light Intensity Search

We implemented the error estimation and search algorithm in hardware. The block diagram is shown in Fig. 10. First, we estimate the error defined in the previous subsection with the structured-light decoding result. To estimate error, SL_ERROR_ESTIMATOR module reads the results of decoding (referred to as "sl_decoding_result") stored in the external memory. Next, OPTIMAL_LIGHT_INTENSITY_SEARCHER module searches for the optimal light-intensity with the input signals (i.e., E_{total}_valid and E_{total}) generated by SL_ERROR_ESTIMATOR module. Our system mounts DMD module that uses LED as a light source. The selected light intensity value is transmitted to the PWM generator module, and the light intensity is regulated by the PWM .

Fig. 11 exhibits SL_ERROR_ESTIMATOR module to acquire the result of Eq. (11).

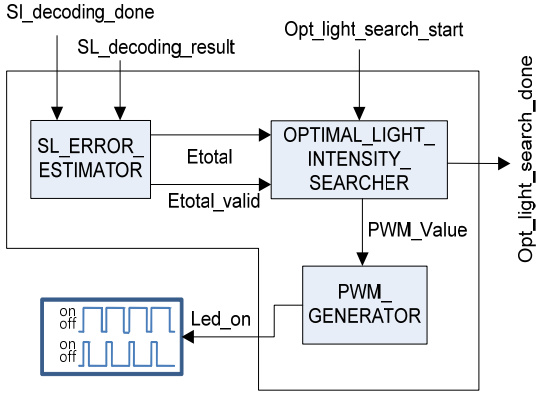

Fig. 10. Light intensity search subsystem.

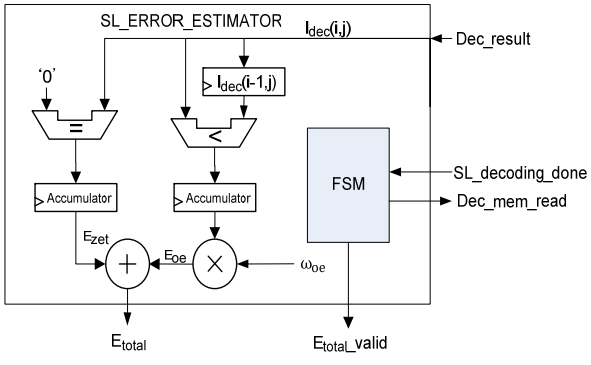

Fig. 11. Error estimator hardware.

IV. Implementation and Experimental Results

1. Hardware Environment and Implementation

Our proposed system is designed in a circuit board (except for DMD interface). Overall architecture is designed in Verilog-HDL and implemented in an FPGA device (Virtex-5) with operating at 50 MHz. The conventional system is configured with an off-the-shelf camera, an off-the-shelf projector, and general PC. After implementing with hardware for entire system, we could remove several limitations from the conventional systems to obtain real time operation. Moreover, conventional systems are limited to the low-flame-rate camera (generally 30~60 fps) whose frame rate of range image is very low (max. 3 fps, required 17frames to yield one range image). Whereas, our solution uses high-speed CMOS image-sensor (500 fps) to increase the frame rate of range image. Furthermore, conventional systems are limited to the low-frame-rate projector (generally 60 fps) whose range image frame rate is very low (max. 3 fps). To overcome the frame rate limitation of projectors, we extract the DMD from projector. Another challenge for the conventional system is synchronization difficulties between camera and projector to capture projected pattern-illuminated image. Due to the hardware and software component synchronization problem, conventional system requires additional hardware circuit, yielding low frame rate. However, our hardware platform approach could resolve the synchronization problem without area overhead and frame rate loss. Table 1 shows the comparison of processing time between our system and conventional system.

As shown in Table 1, our approach is faster by 30

Table 1. Comparison of Processing Time & Frame Rate

Process	Conventional systems [1, 7]	Proposed system
Image acquiring frame rate	60 fps	500 fps
Structured-light projection frame rate	60 fps	500 fps
Decoding	813 ms(1.23 fps)	56 ms(17.85 fps)
Ray-Plane Intersection	928 ms(1.07 fps)	58 ms(17.24 fps)
Total	1741 ms(0.57 fps)	58 ms(17.24 fps)

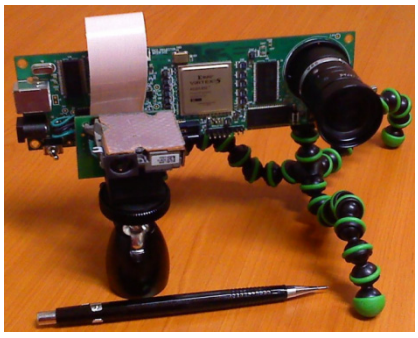

Fig. 12. System board.

times compared to the conventional system configuration. Fig. 12 shows the entire system board that is smaller than the system with using off-the-shelf projector and camera.

2. Experiments on structured light range search

Fig. 13 shows a non-illuminated general image captured by CMOS image-sensor. To evaluate our system, we stacked several objects (a book, two boxes and a paper cup from bottom to top) at a distance of about 50cm from the acquisition system. Notice that the box right below the paper cup is placed diagonally so as to experimentally verify the smooth increase or decrease in distance.

Fig. 14 shows the structured-light decoded image. Each pixel's intensity value represents the column number of the DMD projected image. The black-colored pixel is the invalid value due to either ambiguous correspondences or being out of sight from the projection area. The intensity values of the image pixel is smoothly increased in the right direction, implying that the column numbers of the DMD projected image are increased from left to right.

The range image is shown in Fig. 15. Each pixel's intensity represents the range (in millimeter, the larger value is the nearer position from the acquisition system). The distance values of the 3D points of the diagonally positioned box was smoothly increased or decreased with the front edge of the box as a center. Also note that the distances of the paper cup and the box at the bottom are similar.

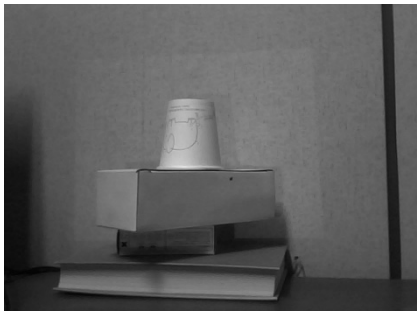

Fig. 13. Non-illuminated image.

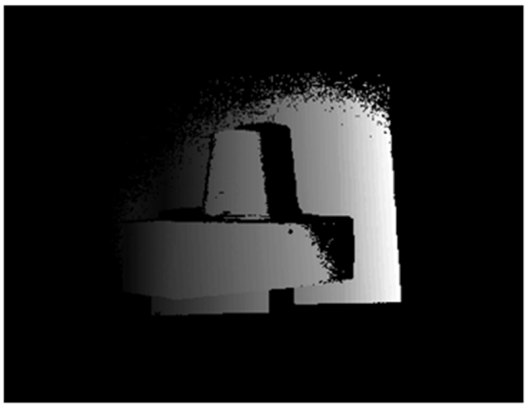

Fig. 14. Structured-light decoding image.

Fig. 16 shows the reconstruction of the objects with the 3D points without any further post processing such as smoothing.

For the purpose of accuracy analysis of our system, we placed a white plane board at a distance of about 60 cm from the acquisition system. First, we obtain 3D points of the white plane through our acquisition system. Next, we reconstructed a flat 3D plane derived from the acquired 3D points using a plane-fitting such as PCA (Principle component analysis). The difference in distance between the points in flat plane and the 3D points is used as a metric for the range accuracy (expressed in terms of average error and standard deviation). Table 2 shows the

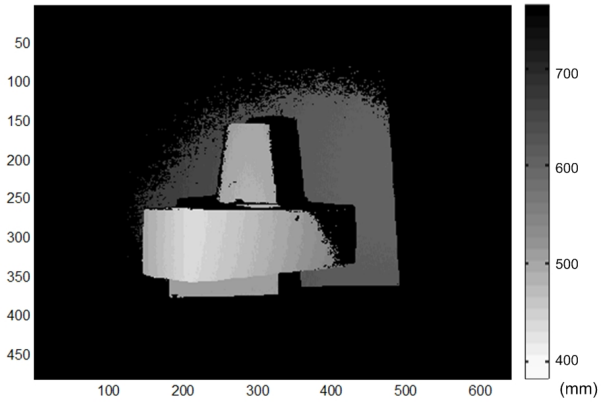

Fig. 15. Range image.

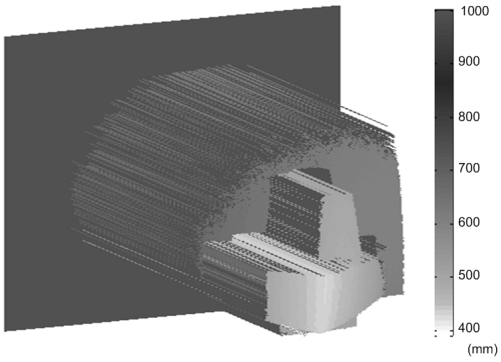

Fig. 16. 3D reconstruction image.

Table 2. System accuracy result

Average error(mm)	Standard deviation(mm)
1.28	0.62

verified result (an average of 10 experiments). This result is reasonable for robot applications.

3. Experiments on light intensity search

We tested our algorithm using the scene shown in Fig. 13. Table 3 compares the total-errors derived from optimal light intensity with the ones from the arbitrary light intensity such as maximum(100%), middle(60%), and minimum(20%) light intensity. The total-error was reduced by 16% compared to the average case .

The *zero-error* represents the number of 3D points and the *order-error* implies the unreliable 3D points. Therefore, we adaptively apply the optimal light intensity to maximize the number of 3D points and accuracy. To show the quality of the measured distance, we set the ROI (Region of Interest) which is flat area in the scene as shown in Fig. 17. Then, we fit a 3D plane in the ROI and compute the accuracy at the arbitrary light intensity and optimal light intensity.

Table 4 shows the number of 3D points in entire image

Table 3. Comparison of decoding errors among different light intensity assignments

Arbitrary γ		O_γ	
γ(%)	$E_{total}(\gamma)$	γ(%)	$E_{total}(\gamma)$
max(100)	0.92	50	0.78
mid(60)	0.87		
min(20)	0.99		

* γ (light intensity), O_γ (optimal light intensity), $E_{total}(\gamma)$ (total error)

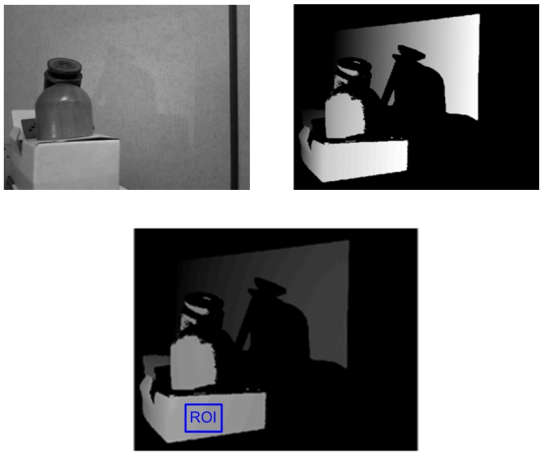

Fig. 17. Test scene & Result images.

Table 4. Comparison of range quality among different light intensity assignments

Light Intensity		Error	Range quality	
A_γ	γ(%)	$E_{total}(\gamma)$	3D points	Average error(mm) in ROI
	max(100)	0.89	21504	2.37
	mid(60)	0.81	49152	1.97
	min(20)	0.92	18432	1.29
O_γ	45	0.72	93501	1.33

* γ (light intensity), A_γ (Arbitrary light intensity), O_γ (optimal light intensity), $E_{total}(\gamma)$ (total error)

area and the accuracy in ROI area at the different light intensity assignment, respectively. The optimal light intensity yields five times more 3D points compared to the worst case(γ=20) with small accuracy reduction (0.04 mm).

We also verified the influence of ambient-light conditions on the optimal-light-intensity of the system. Fig. 18 shows the relationship between $E_{total}(\gamma)$ and structured- light intensity with varying ambient-light

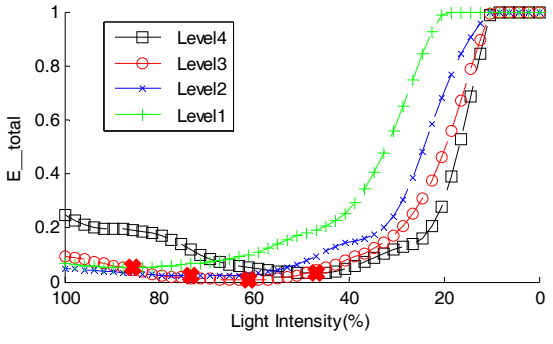

Fig. 18. Influence of ambient light.

conditions. In Fig. 18, the higher level implies higher ambient-light conditions. With our error-model based on $E_{total}(\gamma)$, our system attempts to minimize $E_{total}(\gamma)$ regardless of changed ambient-light condition.

V. CONCLUSIONS

In this paper, we proposed a new technique for the structured-light based range sensing system that is capable of processing of structured-light projection and range computation. Overall processing is realized with fully hard-wired manner using an FPGA that results in real-time operation. The frame-rate of 17 fps (640x480) is reliable in the dynamic scene and feasible to recognize moving objects. Furthermore, to enhance the quality of range sensor and minimize the decoding error, using a proper light intensity leads to desirable results.

Finally, we are posing some future works. First, the current system has room for hardware optimization with pipelining optimization [10] and rescheduling the processes. Second, we might apply various structured-light encoding techniques to secure more robustness with the moving scenes or more accuracy the range data depending on the different conditions.

ACKNOWLEDGMENTS

This research is supported by the Basic Science Research Program through the National Research Foundation of Korea (NRF) funded by the Ministry of Education, Science and Technology(S-2011-0251-000).

REFERENCES

[1] J. Salvi, S. Fernandez, T. Pribanic, and X. Llado, "A state of the art in structured light patterns for surface profilometry," *Pattern Recognition*, Vol.43, No.8, pp.2666-2680, 2010.

[2] S. Zhang, "Recent progresses on real-time 3D shape measurement using digital fringe projection techniques," *Optics and Lasers in Engineering*, Vol.48, No.2, pp.149-158, 2010.

[3] F. Tsalakanidou, F. Forster, S. Malassiotis, and M. G. Strintzis, " Real-time acquisition of depth and color images using structured light and its application to 3D face recognition," *Real-Time Imaging*, Vol. 11(5-6), pp.358-369, 2005.

[4] http://en.wikipedia.org/wiki/Structured-light_3D_scanner.

[5] J. Salvi, J. Pagés, and J. Batlle., "Pattern Codification Strategies in Structured Light Systems," *Pattern Recognition*, Vol.37, No.4, pp.827-849, 2004.

[6] Thomas P. Koninckx, Luc Van Gool, "Real-Time Range Acquisition by Adaptive Structured Light," *IEEE Transactions on Pattern Analysis and Machine Intelligence*, Vol.28, No.3, pp.432-445, 2006

[7] Yi Xu, Daniel G. Aliaga, "An Adaptive Correspondence Algorithm for Modeling Scenes with Strong Interreflections," *IEEE Transactions on Visualization and Computer Graphics*, Vol.15, No.3, pp.465-480, 2009.

[8] D. Scharstein and R. Szeliski, "High-accuracy stereo depth maps using structured light," CVPR03, pp.195-202, 2003.

[9] S. Zhang, P. Huang, "Novel method for structured light system calibration," *Optical Engineering*, Vol.45, No.28, pp.083601, 2006.

[10] Chanho Lee, "Smart Bus Arbiter for QoS control in H.264 decoders," *Journal of Semiconductor Technology and Science*, Vol.11, No.1, pp.33-39, 2011.

Byung-Joo Hong received the B.S. degree in the Department of Electronic Engineering from Dongguk University, Seoul, Korea, in 2005 and the M.S. degree in the Department of Electronic and Electrical Engineering from Sungkyunkwan University, Suwon, Korea, in 2007. He is currently pursuing the Ph.D. degree in the same university. His research interests include 3D image processing and system-on-chip design.

Chan-Oh Park was born in Korea, in 1986. He received the B.S. degree in department of electronic and information engineering from Seoul National University of Technology in 2010. He is currently pursuing the M.S. degree in Sungkyunkwan University. His current research interests include stereo vision, computer architecture and system on chip.

Nam-Seok Seo was born in Korea, in 1982. He received the B.S. degree in department of System Control engineering from Hoseo University in 2009. He is currently pursuing the M.S. degree in Sungkyunkwan University. His current research interests include stereo vision, computer architecture and system on chip.

Jun-Dong Cho received the B.S. degree from the Department of Electronic Engineering, Sungkyunkwan University, Suwon, Korea, in 1980, the M.S. degree from the Department of Computer Science, Polytechnic University Brooklyn, New York, in 1989, and the Ph.D. degree from the Department of Computer Science, Northwestern University, Evanston, in 1993. He was a CAD engineer and Team Leader in Samsung Electronics Company, from 1983 to 1987, and a Senior Technical Staff in Samsung Electronics Company, from 1993 to 1995. In 1995, he joined the Department of Electrical and Computer Engineering, Sungkyunkwan University (SKKU), Suwon, Korea, where he is currently Professor. His research interests include Low Power Design, 3-D Image Processor, Embedded System Integration Design, and Multiprocessor on Chip for Software Defined Radio and Multimedia Applications. Prof. Cho is an IEEE Senior Member.